

IDENTIFICATION OF THE IMPACT OF BLOWING ON THE AERODYNAMIC MODEL OF AN AIRPLANE WITH DISTRIBUTED ELECTRIC PROPULSION

Stefano Cacciola¹, Luca Bottá¹, Carlo E.D. Riboldi¹ & Lorenzo Trainelli¹

¹Department of Aerospace Science and Technology, Politecnico di Milano, Via La Masa 34, 20156 Milano, Italy.

Abstract

This work deals with the identification of the aerodynamic properties of the SwitchMaster, a scaled Distributed Electric Propulsion demonstrator (DEP) aircraft, designed and assembled at Politecnico di Milano, to display the AeroSwitch concept, i.e. the combination of distributed electric propulsion (DEP) configuration and different propulsive control logics that allow replicating in-flight behavior of a single-engine or a twin-engine airplane. The demonstrator has a wingspan of 2.133 m, weighs 4.948 kg and features an array of 6 propellers mounted on the wing's leading edge. After the first flight testing campaign in 2021, dedicated to the demonstration of the concept, a second one was successfully executed in 2023, with the aim of estimating the longitudinal and lateral-direction stability and control derivatives of the SwitchMaster. In this second campaign, a focus was placed on modeling the impact of blowing on the stability and control derivatives. The preliminary results related to the longitudinal dynamics obtained during this identification campaign represent the object of this paper.

Keywords: Distributed Electric Propulsion; System Identification; Blowing; Flight Mechanics; Aerodynamics

1. Introduction

With the aim of improving the sustainability, flexibility, and performance of the next-future aviation systems, electric and hybrid-electric propulsion systems are gaining great attention both in industry and academia [1, 2]. The research on electric aircraft goes together with cutting-edge design concepts, featuring a strong airframe-propulsion integration, such as distributed electrical propulsion (DEP). The DEP configuration, in which a relatively high number of propellers are mounted in front of the leading edge of the wing, is characterized by numerous advantages, such as shorter takeoffs and landings, obtained through blown-lift interactions. In general, it is possible to say that DEP airplanes feature the possibility to exploit the redundancy in the thrust effectors in different flight phases [6, 7]. In 2020, a Politecnico di Milano team was awarded 1st place in the AIAA Graduate Student Aircraft Design Competition thanks to a Distributed Electric Propulsion (DEP) concept, named AeroSwitch. devised to address the problem of reducing the costs associated with flight training for both singleengine and multi-engine operations[3, 4]. In a nutshell, the AeroSwitch concept combines a distributed electric propulsion (DEP) configuration with a set of propulsive control logics allowing the inflight simulation of either a single-engine or a twin-engine airplane. Subsequently, a radio-controlled scaled airplane, named SwitchMaster was designed and built. This model airplane, see Fig. 1, features a wingspan of 2.133 m, weighs 4.948 kg, and is characterized by an array of 6 propellers, mounted on the leading edge of the wing.

Even though it is simple to envision possible applications of the DEP, that can be studied through the SwitchMaster, in this work we consider the aerodynamic modeling of such a system, which is far from being trivial, due to the intrinsically complex interaction among the flow, blown by the propellers, and the lifting surfaces, as witnessed in benchmark conducted in [8]. Moreover, capturing the relevant



Figure 1 – The SwitchMaster model airplane.

physics underlying the aero-propulsive interaction in DEP airplanes is essential when it comes to providing design procedures, able to exploit the advantages of such a configuration [9, 10].

In a first attempt to generate an aerodynamic model of the SwitchMaster, the software Xplane was employed. Although this tool typically provides realistic modeling of conventional aircraft, it delivered mixed results in the case analyzed here.

For this reason, we decided to develop a flight mechanics model based on the widespread stability and control (S&C) derivatives, suitably adapted for the DEP case.

In particular, we followed a two-pronged approach. Firstly, we set up a vortex-lattice model of the Switch Master through the software OpenVSP [5], in which the propellers are modeled as actuator disks. Although OpenVSP may offer a fast and complete aerodynamic characterization, including the desired stability and control derivatives, we employed this tool only to obtain a qualitative idea of the trend of the S&C derivatives as functions of a parameter related to the blowing level, i.e. the propeller advance ratio J, defined as

$$J = \frac{V}{nD},\tag{1}$$

where V is the airplane speed, n is the propeller rotational speed, expressed here in revolutions-perseconds, and D is the propeller diameter. Notice that the unblown condition, i.e. considering all idling engines, characterized by n=0, implies $J\to\infty$. For this reason, the unblown case will be hereafter associated with an infinite advance ratio. From OpenVSP results, we noticed that most of the S&C derivatives feature an exponential behavior with respect to the advance ratio.

Afterward, the parameters describing the exponential behavior of stability and control derivatives were estimated from dedicated flight experimentation through the standard identification procedures based on maximum likelihood.

The testing campaign carried out between March and April 2023 comprised multiple pitch maneuvers generated through suitable motions of the elevator. In order to suitably excite the longitudinal response of the machine, and in particular the short period mode, part of the testing campaign was dedicated to the selection of the appropriate amplitude and duration of the elevator perturbation. Due to their lower complexity, doublets were preferred to more sophisticated perturbations, e.g. frequency sweep or 3–2–1–1 inputs, so as to ease the testing execution.

Each test was repeated multiple times for different throttle levels, including idle, to generate blowing of various magnitudes.

Even if part of the experimentation also considered roll and yaw maneuvers, conducted for the estimation of the lateral-directional parameters, in this paper, we will focus only on the longitudinal S&C derivatives and the quantification of the blowing impact on such quantities. The extension of the present work to the lateral-directional plane is currently in progress.

The present paper is organized as follows. Section 2. deals with the description of the methodology employed in this work and is broken into four parts. The preliminary investigation conducted through <code>OpenVSP</code> is the object of Sec. 2.1 the definition of the exponential function that models the blowing

impact on S&C derivatives is presented in Sec. 2.2; the testing procedures, along with a thorough description to the Switch Master and its sensing equipment, is described in Sec. 2.3, whereas Sec. 2.4 deals with a brief review of the system identification techniques based on maximum likelihood methodology. The results of the estimation of the longitudinal S&C derivatives are the object of Section 3. Finally, the main findings and the lessons learned from this first experimental campaign are summarized in Sec. 4.

2. Methodology

2.1 Preliminary investigation on the aerodynamics of a distributed electric propulsion demonstrator through OpenVSP

The model of the *SwitchMaster*, created in OpenVSP, includes the propellers in front of the wing as actuator disks. Some simplifications in the model geometry were made due to the complex shape of the airplane and to avoid numerical issues. In particular, wing and tail tips were neglected, while the geometry of the elevator and rudder was simplified, providing that the related area remained unaltered. Moreover, the fuselage cross-sections, which in the real demonstrator are rectangular with rounded corners, were modeled through ellipses with the same height and width. Finally, engine nacelles and landing gears were not included. Such a model, although simplified, is considered adequate to qualitatively capture the impact of blowing on the aerodynamic derivatives. A convergence study was also conducted to select suitable discretization parameters. The details of this analysis are reported in Ref. [12].

Figure 2 displays a sketch of the demonstrator as implemented in OpenVSP.

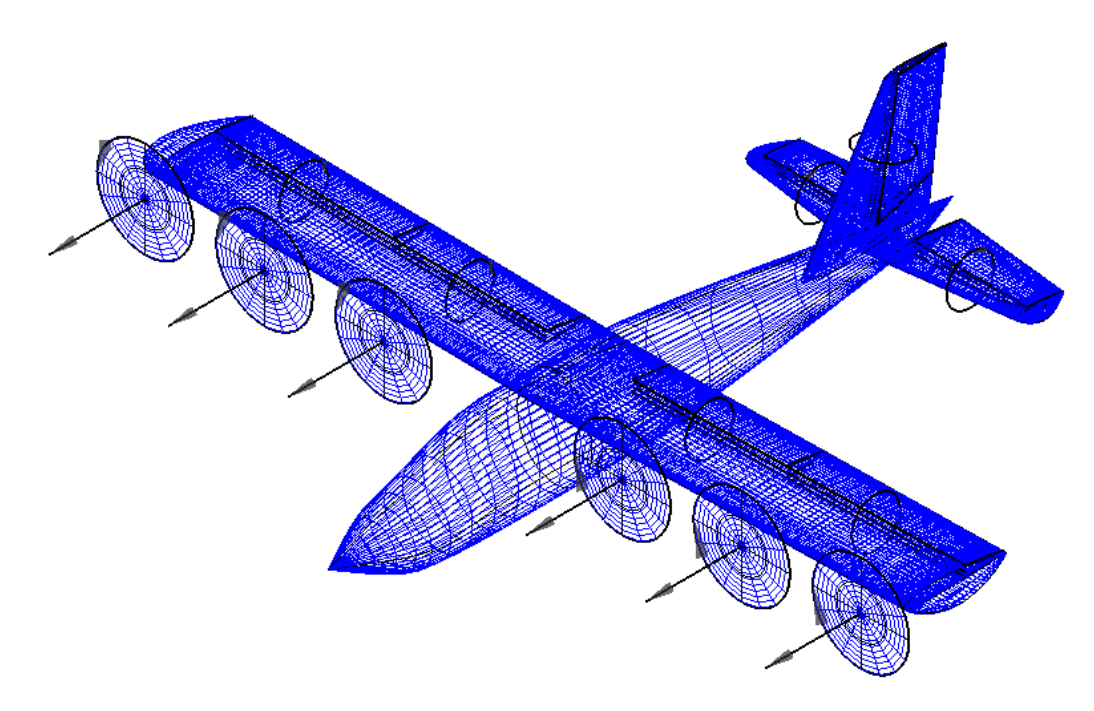


Figure 2 - Model of the SwitchMaster in OpenVSP.

The actuator disk characteristics were defined according to a previous wind tunnel testing campaign, in which the power and thrust of a single full-scale engine-propeller group were measured as functions of the angular velocity of the propeller and wind speed. The details of this experimentation and the corresponding data can be found in Ref. [11].

The OpenVSP analysis focused on a typical flight condition for the SwitchMaster model, i.e. airplane speed equal to $15~\mathrm{m/s}$, angle of attack equal to $5.5~\mathrm{deg}$. The simulations considered nine different values of propeller advance ratio, from J=0.34 to 0.56, along with the unblown condition represented by $J=\infty$. The minimum and maximum values of J were chosen according to those wind tunnel testing conditions where the highest and lowest positive C_T values were experienced.

Figure 3 shows the trends of all longitudinal S&C derivatives as functions of the propeller advance ratio, obtained from the <code>OpenVSP</code> simulations. Blue dots represent the results of the analyses whereas the black-thin dash-dotted horizontal lines refer to the unblown values for each derivative, which is also reported in correspondence of $J = \infty$. The solid red curves refer to the exponential fit of the kind $y = A e^{BJ} + C$, whose coefficients A, B have been computed for each derivative through least-squared, while coefficient C has been set equal to the value of the unblown coefficient. To better interpret the results, the subplots of Fig. 3 are organized so that the three columns refer respectively to the derivatives of the lift coefficient C_L , of the drag coefficient C_D and of the moment coefficient about the center of gravity C_m , whereas the four rows are related to the constant terms (first row) to the derivatives with respect to the angle of attack α (second row), to the derivatives respect the non dimensionalized pitching moments $\hat{q} = q \, c / (2 \, \mathcal{V})$ being q the dimensional pitching moment, c mean aerodynamic chord and \mathcal{V} the airplane speed (third row). Finally, the fourth row is associated with the derivative with respect to the elevator deflection δe .

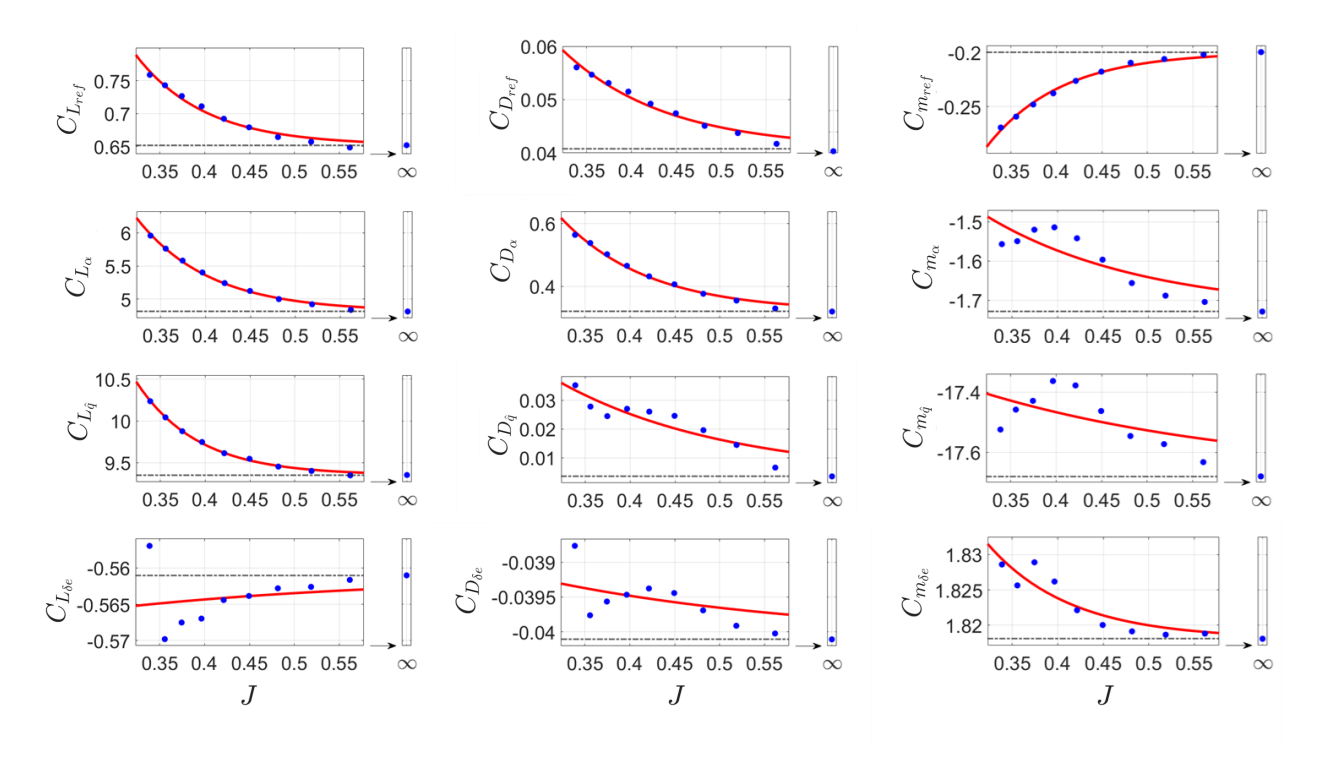


Figure 3 – Logitudinal S&C derivatives estimated through OpenVSP. Blue dots: simulation results; Solid red curve: exponential fit; thick dash-dotted line: unblown values.

From the obtained graphs, it seems that the majority of the S&C derivatives feature an exponential trend that converges to the unblown value as J becomes larger, i.e. as J approaches ∞ .

In particular, the exponential function is accurate for $C_{L\alpha}$, $C_{D\alpha}$, $C_{L\hat{q}}$ and for all constant coefficients, $C_{L\mathrm{ref}}$, $C_{L\mathrm{ref}}$, and of $C_{L\mathrm{ref}}$. Moreover, the agreement is acceptable, although not perfect, for $C_{D\hat{q}}$, $C_{m\delta e}$ and $C_{m\alpha}$.

The other derivatives, whose behavior deviates more from the ideal exponential trend, are however mildly affected by blowing, i.e. $C_{L\delta e}$, $C_{D\delta e}$ and $C_{D\hat{a}}$.

From this preliminary analysis, we can conclude that, at least in the first approximation, the impact of blowing on S&C derivatives can be modeled through exponential functions dependent on the propeller advance ratio.

2.2 Extending the standard stability and control derivatives to include the blowing effect

The crucial aero-propulsive interaction between the downstream flow of the propellers and the lifting surfaces is taken into account by considering in the usual stability and control derivatives a dependency on the collective propeller advance ratio *J*. Modeling this effect in a simple but accurate way is far from being trivial as witnessed by the analytical formulation provided by Patterson et al. [13].

Moreover, complicated relationships also entail sophisticated processes to tune the related parameters that often require a significant amount of data.

However, as we have shown in Sec. 2.1, it is possible to preliminary model the blowing impact on S&C derivatives in a rather simple way through exponential functions dependent on J.

To this end, each aerodynamic derivative is modeled as the sum of two contributions; the first represents the unblown coefficient, i.e. that characterizing the airplane with null thrust, while the second captures the dependency on the blowing, as

$$C_{\xi_{\mathcal{U}}}(J) = C_{\xi_{\mathcal{U}}}^{\text{unbl}} + \Delta C_{\xi_{\mathcal{U}}}(J)$$
(2)

where $C_{\xi_{\mu}}$ represents the derivative of the coefficient of force (or moment) ξ with respect to the variable μ . The superscript "unbl" refers to the unblown part, while $\Delta C_{\xi_{\mu}}(J)$ is the variation of the coefficient that depends on the advance ratio J, which is modeled through an exponential function as

$$\Delta C_{\xi_{\mu}}(J) = A_{\xi,\mu} e^{B_{\xi,\mu}J} \tag{3}$$

Consequently, the derivative of the aerodynamic coefficient ξ with respect to variable μ is described through three unknown coefficients, the unblown part $C_{\xi}_{\mu}^{\text{unbl}}$, and two parameters defining the exponential terms A_{ξ}_{μ} and B_{ξ}_{μ} .

nential terms $A_{\xi,\mu}$ and $B_{\xi,\mu}$. The three parameters $C_{\xi_{\mu}^{unbl}}$, $A_{\xi,\mu}$ and $B_{\xi,\mu}$, describing the empirical relationship between each S&C derivative and J, cannot be analytically evaluated, but shall rather be estimated from the values of the derivatives $C_{\xi_{\mu}}(J)$ at different advance ratios. Section 2.4 will detail the mathematical formulation for estimating these variables from flight data. In this process, it is also important to consider a test with idling propellers that can be used for directly estimating the unblown coefficient $C_{\xi_{\mu}^{unbl}}$ and, in turn, for evaluating $\Delta C_{\xi_{\mu}}(J)$.

Finally, coefficients $A_{\xi,\mu}$ and $B_{\xi,\mu}$ are easily computed by fitting the values $\Delta C_{\xi,\mu}(J)$ with an exponential function.

2.3 Experimental campaign: definition of the test matrix and measurement equipment

In order to identify the longitudinal aerodynamic derivatives of the model and their dependency on the advance ratio, a large number of maneuvers were carried out, mainly consisting of short-period excitation through pitch doublets. Pull-up, push-over and phugoid tests were also performed, to gather additional data, which could be employed for validation or, in general, for further developments of the model.

In this first campaign, to simplify the estimation process and focus on the sole impact of the blowing, the tests were performed with collective control of engines, at speeds between 15 and $20~\mathrm{m/s}$. Moreover, while maintaining the selected speed, the tests were repeated changing the throttle value, so as to operate the airplane at different advance ratios. This process implied that the airplane needed to be trimmed with different flight path angles γ . For example, at low J the SwitchMasted flew with γ equal to about $40~\mathrm{deg}$.

As already mentioned in Sec. 2.2, some tests were also performed in idling conditions to provide data to identify the unblown model and, consequently, estimate the coefficients $\Delta C_{\xi_{\mu}}(J)$ as reported in Eq. (2).

A total of 30 pitch doublet maneuvers were performed, which are used for identification and validation purposes. In particular, 3 doublets were accomplished in idling condition, with $J \to \infty$. One of these maneuvers was used for identifying the unblown S&C derivatives, while the other two were employed for validation. The remaining 27 tests were performed in different conditions spanning different values of α from -7 to 12 deg, different flying speeds V from 13 to 21 m/s and various values of propeller advance ratios J from 0.31 to 0.53. Among these 27 tests, 22 were used for identification and 5 for validation purposes.

The measuring equipment of the SwitchMaster consists of the following sensors:

• Pitot tube and thermometer, located at the nose of the airplane, sensing the static and total pressure as well as outside air temperature, all recorded at 100 Hz;

Identification of the Impact of Blowing on the Aerodynamics of a Distributed Electric Propulsion Demonstrator

- GPS, located close to the center of gravity of the airplane, sensing the position of the airplane recorded at 50 Hz;
- Inertial unit, located close to the center of gravity of the airplane, sensing the accelerations in a body reference a_x , a_y and a_z , that are recorded at 20 Hz, angular rates, p, q and r, again in the body reference, that are recorded at 300 Hz and attitute angles ϕ (roll), θ (pitch) and ψ (heading), that are recorded at 20 Hz;
- One encoder on each control surface, sensing the related deflection recorded at 200 Hz.
- One encoder on each engine shaft, sensing the related rotation velocity recorded at 4 Hz.

All measurements were low-pass filtered to avoid aliasing and resampled at $20~\mathrm{Hz}$. The density of the air ρ is computed from static pressure and outside air temperature. The indicated airspeed (IAS) is calculated as usual from the static and total pitot ports. The calibrated airspeed (CAS) is then retrieved from IAS through a calibration function found through a dedicated wind tunnel experimentation. Since the velocities potentially flyable are low, the IAS can be safely considered equal to the equivalent airspeed (EAS). True airspeed (TAS) is finally recovered from EAS and air density. The altitude h is provided by GPS as well as the airplane position.

The measurements of the aerodynamic angles, angle of attack α and side-slip angle β , are estimated by combining the GPS signals, the attitude angles and an on-ground wind measurement. In particular, let us indicate with $\mathbf{V}^{\mathscr{N}}$ the components of airplane speed in NED (North-East-Down) frame, computed by time-derivating the GPS positions, and with $\mathbf{V}^{\mathscr{N}}_{\mathrm{w}}$ the components of the wind in the NED frame measured by an on-ground anemometer. Notice that, as customarily done, when dealing with vectors, we indicate in the superscript the frame in which we express its components.

At first, the components in frame \mathscr{N} of the airplane velocity relative to the surrounding air, noted $V_{\mathrm{AS}}^{\mathscr{N}}$, are computed as

$$V_{\rm AS}^{\mathcal{N}} = V^{\mathcal{N}} - V_{\rm w}^{\mathcal{N}}. \tag{4}$$

Then, one can easily change the basis of the components of V_{AS} from the NED to the body frame

$$\boldsymbol{V}_{\mathrm{AS}}^{\mathscr{B}} = \left(R_{\mathcal{N}\to\mathscr{B}}^{\mathscr{N}}\right)^{T} \boldsymbol{V}_{\mathrm{AS}}^{\mathscr{N}},\tag{5}$$

where

$$R_{\mathcal{N}\to\mathcal{B}}^{\mathcal{N}} = \begin{bmatrix} \cos\psi\cos\theta & \cos\psi\sin\theta\sin\phi - \sin\psi\cos\phi & \cos\psi\sin\theta\cos\phi + \sin\psi\sin\phi \\ \sin\psi\cos\theta & \sin\psi\sin\theta\sin\phi + \cos\psi\cos\phi & \sin\psi\sin\theta\cos\phi + \cos\psi\sin\phi \\ -\sin\theta & \cos\theta\sin\phi & \cos\theta\cos\phi \end{bmatrix}$$
(6)

is the rotation tensor that transforms $\mathscr N$ triad into $\mathscr B$, with components expressed in $\mathscr N$. From the components of the velocity in $\mathbf V_{\mathrm{AS}}^{\mathscr B}=\{U,V,W\}^T$, being U,V and W respectively the longitudinal, lateral and vertical components, the values of α and β are readily computed as

$$\alpha = \arctan\left(\frac{W}{U}\right)$$

$$\beta = \arcsin\left(\frac{V}{\sqrt{U^2 + V^2 + W^2}}\right)$$
(7)

2.4 Identification of the longitudinal derivatives of the through SwitchMaster from flight data

The estimation of the stability and control derivatives for each maneuver was performed through the standard equation- and output-error approaches [14]. In the following, we briefly review these estimation techniques highlighting the peculiarities encountered while applying such methodologies to the SwitchMaster experimental data.

2.4.1 Identification through the equation error method

The equation error is a regression method that can be solved in closed form (see Ref. [14], Chapter 4). In particular, the time histories of lift C_L , drag C_D and pitch moment about the center of gravity C_m coefficients can be computed by recasting the standard longitudinal equations of motion as

$$C_L(t) = -C_Z(t)\cos\alpha(t) + C_X(t)\sin\alpha(t)$$
(8a)

$$C_D(t) = -C_X(t)\cos\alpha(t) - C_Z(t)\sin\alpha(t)$$
(8b)

$$C_m(t) = \frac{1}{\overline{q}(t)Sc} [I_y \dot{q}(t) + (I_x - I_z)p(t)r(t) + I_{xz}(p^2(t) - r^2(t)) - I_p \Omega_p r(t)]$$
(8c)

where the longitudinal and vertical coefficients of the aerodynamic force in the body frame, noted C_X and C_Z , are

$$C_X(t) = \frac{1}{\overline{q}(t)S}(ma_X(t) - T(t))$$
(9a)

$$C_Z(t) = \frac{m a_z(t)}{\overline{q}(t)S},\tag{9b}$$

S is the wing area, c is the mean aerodynamic chord, m the mass of the airplane, $\overline{q} = \frac{1}{2}\rho(t)\mathcal{V}^2(t)$ indicates the dynamic pressure, I_x , I_y , I_z and I_{xz} are the components of the symmetric inertia tensor of the airplane in the body frame with longitudinal, lateral and vertical axes indicated with x, y and z. Moreover, I_p and Ω_p are respectively the overall propeller inertia about the rotor axis and the propeller rotational speed, included here to model the gyroscopic moments due to the propellers themselves, and T is the total engine thrust computed from a thrust model previously derived through wind tunnel tests (as already explained in Sec. 2.1).

The relationships between the aerodynamic coefficients and the airplane variables are then formulated through the standard S&C derivatives as

$$C_L(t) = C_{Lref} + C_{L\alpha}(\alpha)\alpha(t) + C_{L\hat{\alpha}}\hat{q}(t) + C_{L\delta e}\delta e(t)$$
(10a)

$$C_D(t) = C_{Dref} + C_{D\alpha}(\alpha)\alpha(t) + C_{D\hat{\alpha}}\hat{q}(t) + C_{D\delta_e}\delta e(t)$$
(10b)

$$C_m(t) = C_{mref} + C_{m\alpha}(\alpha)\alpha(t) + C_{m\hat{\alpha}}\hat{q}(t) + C_{m\delta e}\delta e(t). \tag{10c}$$

The derivative of the coefficients with respect to α , indicated with $C_{D\alpha}(\alpha)$, is here made dependent on α itself. This is expected to be important for C_D to capture the expected parabolic behavior of the drag. Focusing on drag, one may write

$$C_{D\alpha}(\alpha)\alpha = (f_1 + f_2\alpha)\alpha = f_1\alpha + f_2\alpha^2, \tag{11}$$

where f_1 and f_2 are two coefficients of the linear expansion of the $C_{D\alpha}(\alpha)$.

To simplify the treatment, with a certain abuse of notation, we will refer to f_1 and f_2 respectively as $\tilde{C}_{D\alpha}$ as $\tilde{C}_{D\alpha^2}$, that now represent two parameters to be identified within the set of the S&C derivatives. Equation 10b then reads

$$C_D(t) = C_{Dref} + \tilde{C}_{D\alpha}\alpha(t) + \tilde{C}_{D\alpha^2}\alpha^2(t) + C_{D\hat{\alpha}}\hat{q}(t) + C_{D\delta e}\delta e(t)$$
(12)

Formally similar equations, not reported here for the sake of brevity, can also be derived for lift and moment coefficients.

Notice that in Eq. 10, we have neglected the dependency of the aerodynamic forces and moments on the derivatives of the angle of attack $\dot{\alpha}$, due to the reduced dimensions of the airplane.

Let us assume that the indirect measurements of the aerodynamic coefficients, defined in Eq. (8), and the measurements of the aerodynamic variables α , \hat{q} and δe , although affected by noise, obey the aerodynamic model in Eq. (10). To this end, consider the sampled version of all flight mechanics measured variables and indicate the time index with $k=1,\ldots,N$. Consequently, Eqs. (10) can be

written for each instant of time as

$$\begin{cases}
C_{\xi_{m}}(1) \\
C_{\xi_{m}}(2) \\
\vdots \\
C_{\xi_{m}}(k) \\
\vdots \\
C_{\xi_{m}}(N)
\end{cases} =
\begin{bmatrix}
1 & \alpha_{m}(1) & \alpha_{m}^{2}(1) & \hat{q}_{m}(1) & \delta e_{m}(1) \\
1 & \alpha_{m}(2) & \alpha_{m}^{2}(2) & \hat{q}_{m}(2) & \delta e_{m}(2) \\
\vdots & \vdots & \vdots & \vdots & \vdots \\
1 & \alpha_{m}(k) & \alpha_{m}^{2}(k) & \hat{q}_{m}(k) & \delta e_{m}(k) \\
\vdots & \vdots & \vdots & \vdots & \vdots \\
1 & \alpha_{m}(N) & \alpha_{m}^{2}(N) & \hat{q}_{m}(N) & \delta e_{m}(N)
\end{cases}
\begin{cases}
C_{\xi_{ref}} \\ \tilde{C}_{\xi \alpha} \\ C_{\xi_{\alpha}^{2}} \\ C_{\xi_{\alpha}^{2}} \\ C_{\xi_{\delta e}} \end{cases} +
\begin{cases}
\eta(1) \\ \eta(2) \\ \vdots \\ \eta(k) \\ \vdots \\ \eta(N)
\end{cases}$$
(13)

where C_{ξ} is a generic aerodynamic coefficient, i.e. lift, drag or moment, η is noise, considered here white and with variance equal to σ^2 , and the subscript `m' refers to a measured quantity. Equation (13) can be given a more compact form as

$$Z = X\Theta + \eta, \tag{14}$$

being Z an array collecting the samples of the aerodynamic coefficients, Θ an array collecting the unknown S&C derivatives, X the regressor matrix and η an array containing the noise. Notice that matrix X is rectangular with N rows and M columns, being N the number of samples considered and M the number of unknown parameters.

Finally, the solution Θ_{EST} , i.e. the array containing the estimated S&C derivatives, is computed separately for lift, drag and moment coefficients in the least square sense, as

$$\mathbf{\Theta}_{\mathrm{EST}} = \left(\mathbf{X}^T \mathbf{X} \right)^{-1} \mathbf{X}^T \mathbf{Z}. \tag{15}$$

It is possible to demonstrate that, for zero-mean white noise, such an estimator is unbiased, i.e. the expected value of the estimated and real solution coincide and that the covariance of the estimates is equal to

$$var(\mathbf{\Theta}_{EST} - \mathbf{\Theta}) = \sigma^2 (\mathbf{X}^T \mathbf{X})^{-1}.$$
 (16)

The diagonal entries of the variance matrix represent the variance of the estimated quantities in Θ_{EST} . Equation (16) deserves special attention: a too-high variance may indicate an ill-posed problem with inconsistent results. This typically happens when some regressors in matrix X are linearly dependent, leading to an ill-conditioned matrix (X^TX) .

To detect collinearity problems, among all regressors excluding the unitary one (i.e. the first column of matrix X), it is possible to check the so-called correlation matrix C, that is a $(M-1) \times (M-1)$ symmetric square matrix in which each (i, j) element, noted $C_{(i, j)}$, is defined as

$$C_{(i,j)} = \frac{\left(\boldsymbol{\xi}_{(i+1)} - \operatorname{mean}\left(\boldsymbol{\xi}_{(i+1)}\right)\right)^{T} \left(\boldsymbol{\xi}_{(j+1)} - \operatorname{mean}\left(\boldsymbol{\xi}_{(j+1)}\right)\right)}{\operatorname{std}\left(\boldsymbol{\xi}_{(i+1)}\right) \operatorname{std}\left(\boldsymbol{\xi}_{(j+1)}\right)},$$
(17)

where $\pmb{\xi}_\ell$ is the ℓ th column of matrix \pmb{X} and $\{i;j\}=\{1,\ldots,M-1;1,\ldots,M-1\}.$

It is simple to verify that $-1 \le C_{(i,j)} \le 1$ and that all diagonal entries $C_{(i,i)}$ are equal to 1. Each $C_{(i,j)}$ coefficient represents the level of correlation of regressors i and j. In general, $\left|C_{(i,j)}\right| > 0.9$ indicate that regressors i and j are correlated and, in turn, that the two associated parameters cannot be estimated separately. Clearly, the correlation is to be verified among all S&C derivatives excluding the reference coefficients.

2.4.2 Identification through the output error method

The output error approach is based on the minimization of the prediction error between the flight test measurements and simulated outputs (see Ref. [14], Chapter 6).

To this end, consider the longitudinal dynamic equation of motion,

$$\dot{\mathscr{V}} = -\frac{\overline{q}S}{m}C_D + \frac{T}{m}\cos\alpha\cos\beta + g(\cos\phi\cos\theta\sin\alpha\cos\beta + \sin\phi\cos\theta\sin\beta - \sin\theta\cos\alpha\cos\beta)$$
 (18a)

$$\dot{\alpha} = q - \frac{\overline{q}SC_L}{mV\cos\beta} - \tan\beta(p\cos\alpha + r\sin\alpha) - \frac{T\sin\alpha}{mV\cos\beta} + \frac{g}{V\cos\beta}(\cos\phi\cos\alpha\cos\alpha + \sin\theta\sin\alpha) \quad (18b)$$

$$\dot{q} = \frac{\overline{q}Sc}{I_{v}}C_{m} - \frac{(I_{x} - I_{z})}{I_{v}}pr - \frac{I_{xz}}{I_{v}}(p^{2} - r^{2}) + \frac{I_{p}}{I_{v}}\Omega_{p}r$$
(18c)

$$\dot{\theta} = q\cos\phi - r\sin\phi. \tag{18d}$$

For a given set of S&C derivatives organized in vector $\boldsymbol{\theta}$, Eqs. (18) can be used to compute the evolution of \mathcal{V} , α , q and θ , starting from specific initial conditions, noted as \mathcal{V}_0 , α_0 , q_0 and θ_0 . Let us stack, the initial conditions in array \mathbf{y}_0

$$\mathbf{y}_0 = \{ \mathcal{V}_0, \, \alpha_0, \, q_0, \, \theta_0 \}^T. \tag{19}$$

Then, for a generic time index k, the output variables, that depends upon Θ and y_0 , can be collected in array $y(k; \Theta, y_0)$

$$\mathbf{y}(k; \mathbf{\Theta}, \mathbf{y}_0) = \{ \mathcal{V}(k), \alpha(k), q(k), \theta(k) \}^T, \tag{20}$$

while the measured variables in array z

$$\mathbf{z}(k) = \{ \mathcal{V}_{\mathbf{m}}(k), \, \alpha_{\mathbf{m}}(k), \, q_{\mathbf{m}}(k), \, \theta(k) \}^{T}. \tag{21}$$

Define now the residue at time step k as

$$\mathbf{v}(k; \mathbf{\Theta}, \mathbf{y}_0) = \mathbf{z}(k) - \mathbf{y}(k; \mathbf{\Theta}, \mathbf{y}_0)$$
(22)

and cost function $F(\mathbf{\Theta})$

$$F(\mathbf{\Theta}) = \frac{1}{NL} \sum_{k=1}^{N} \mathbf{v}^{T}(k; \mathbf{\Theta}, \mathbf{y}_{0}) \mathbf{R}^{-1} \mathbf{v}(k; \mathbf{\Theta}, \mathbf{y}_{0}),$$
(23)

where L is the number of measures employed for the estimation, i.e. the length of array z(k), whereas R is the covariance matrix of the noise.

According to the output error, the estimation problem is that of finding the unknown Θ that minimizes the cost function $F(\Theta)$. This clearly requires a nonlinear optimization algorithm, seeking the minimum starting from a suitable initial guess on Θ , noted here Θ_{in} .

The initial conditions in y_0 , to integrate Eq. 18, are set by averaging the flight mechanics variables within the first instants of time, before the perturbation.

Each maneuver was identified separately, first with the equation error, as for Sec. 2.4.1. Then, the solution computed with the equation error is given as the initial guess Θ_{in} for the nonlinear optimization required by the more accurate output error approach.

The noise covariance matrix \mathbf{R} , on the other hand, was estimated using the residue associated with the initial guess $\mathbf{\Theta}_{in}$ as

$$\mathbf{R}_{\text{EST}} = \frac{1}{N} \sum_{k=1}^{N} \mathbf{v}(k; \, \mathbf{\Theta}_{\text{in}}, \mathbf{y}_0) \mathbf{v}^T(k; \, \mathbf{\Theta}_{\text{in}}, \mathbf{y}_0). \tag{24}$$

The accuracy level of the estimates can be evaluated for the output error as well. In fact, under the assumption that all measurements are corrupted by zero-mean, uncorrelated and white noise, it is possible to demonstrate that the output error estimator is unbiased and that the estimation variance obeys the Cramér-Rao lower bounds

$$\operatorname{var}(\mathbf{\Theta}_{\mathrm{EST}} - \mathbf{\Theta}) \ge \left(\sum_{k=1}^{N} \left(\mathbf{S}_{k}^{T} \mathbf{R}^{-1} \mathbf{S}_{k}\right)\right)^{-1},\tag{25}$$

where S_k is the sensitivity of the outputs at time step k, noted y(k), with respect to the parameters Θ evaluated at the estimated value,

$$S_k = \frac{\partial y(k)}{\partial \Theta} \bigg|_{\Theta = \Theta_{EST}}$$
(26)

Once the S&C derivatives are estimated for different advance ratios J, including $J = \infty$, it is possible to fit the results through an exponential function, as indicated in Eq. 3.

3. Results

During the test executions and a first data check, it was observed that maintaining the SwitchMaster at trim at the desired condition before the doublet excitation was hard. This was because the model was manually piloted, hence the pilot did not perceive the accelerations to which the system is subjected. In addition, the blowing of the propeller on the aerodynamic surfaces modifies the behavior of the airplane such that the pilot needs to govern a system that is a bit different at every maneuver. Moreover, for the same reason, performing a proper pitch doublet able to suitably excite the short period is not trivial.

Notwithstanding these objective issues, the pilot was able to suitably complete the flight test card and the gathered data were satisfactory for the majority of the tests.

Clearly, an autopilot with a speed and altitude hold mode should be introduced to ease test executions and improve the quality of the flight data.

Data from 22 pitch doublet maneuvers of the 27 performed were used to identify S&C derivatives by applying the equation- and the output-error approaches, as detailed in Sec. 2.4.

Figure 4 shows an example of the matching between flight data and simulated outputs in terms of the aerodynamic coefficients, as a result of the equation error estimation (Sec. 2.4.1). The data refer to a pitch doublet performed at an advance ratio J=0.445. Blue curves represent C_L , C_D and C_m coefficients computed from flight measurements using the Eqs. 10, whereas the yellow and red curves are associated with the identifications performed using two sets of regressors, i.e. including α^2 or not.

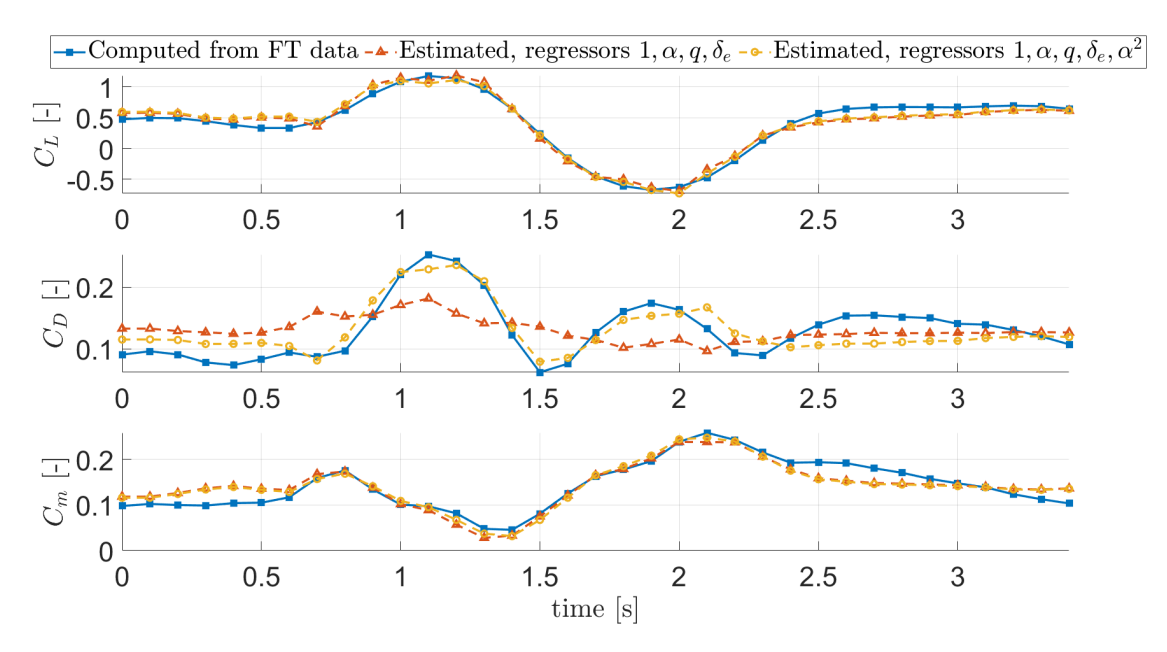


Figure 4 – Agreement between flight and simulated data for a pitch doublet performed at advance ratio J=0.445, using the equation error approach. Top plot: C_L ; middle plot: C_D ; bottom plot: C_m . Blue curves: coefficients extracted from flight data; red curves: estimation using four regressors (α^2 not included); yellow curves: estimation using five regressors (α^2 included).

In general, the matching is quite good for all coefficients. Moreover, as expected, including the α^2 regressor strongly improves the estimation of the C_D , while it does not significantly impact the agreement in terms of C_L and C_D .

Table 1 reports the correlation matrix of the same test. Most of the obtained correlations appear high even if none of the values is greater than 0.9, the threshold commonly used for detecting collinearity problems. The highest value is associated with the correlation between \hat{q} and δe and is equal to 0.8694.

Figure 5 shows, for all tested maneuvers, the correlation coefficient for the couples $\{\alpha, \hat{q}\}$, $\{\alpha, \delta e\}$ and $\{\hat{q}, \delta e\}$, noted respectively $k_{\alpha,q}$, $k_{\alpha,\delta e}$ and $k_{q,\delta e}$, which are displayed versus the advance ratio J. It is possible to notice that $k_{\alpha,\delta e}$ generally represents the lowest correlation coefficient, whereas $k_{q,\delta e}$ is

Table 1 – Correlation matrix of the regressors associated with the identification test of 4

	α	\hat{q}	δe	$lpha^2$
α	1.0000	0.8577	0.5995	-0.8619
\hat{q}		1.0000	0.8694	-0.7898
δe			1.0000	-0.4907
α^2				1.0000

the highest one. Moreover, $k_{\alpha,q}$ and $k_{\alpha,\delta e}$ feature an increasing trend as the J increases, a behavior that deserves further investigation.

Although collinearity issues, with coefficients greater than 0.9, were not reported, the correlation among some regressors is far from being optimal, especially at high J. This indicates that better maneuvers can be performed to improve the goodness of the flight data. For example, automatic systems able to perturb the airplane through more complex and effective inputs, such as frequency sweep or 3-2-1-1, should be considered.

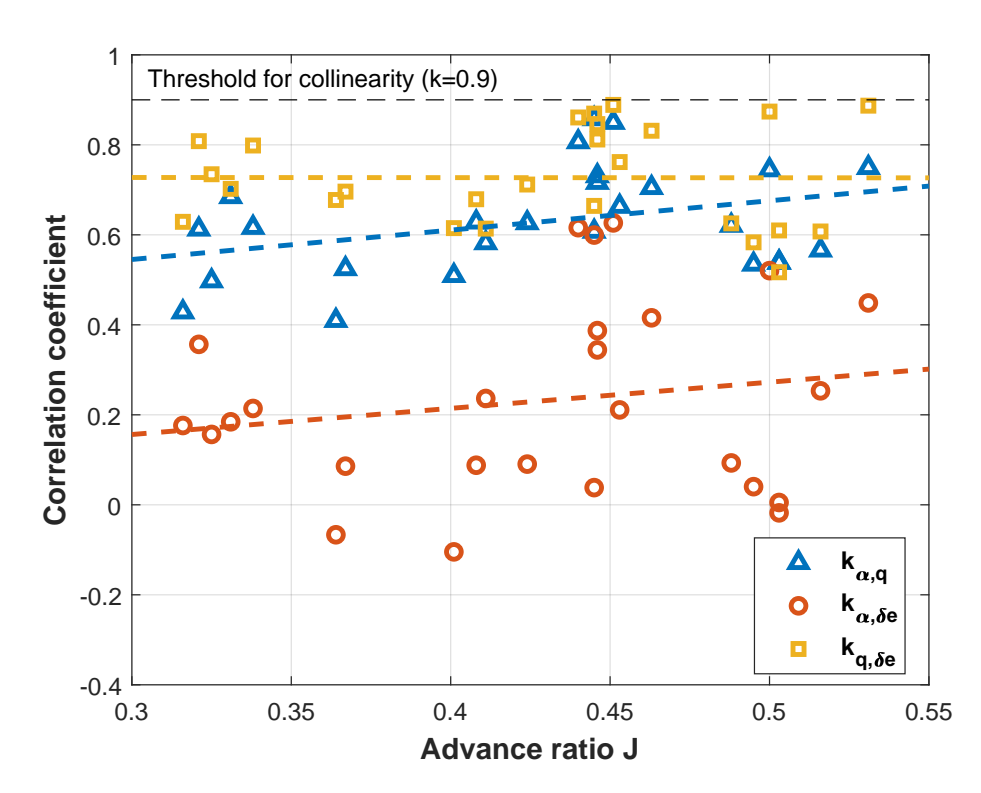


Figure 5 – Trend of the correlation coefficients versus the advance ratio. Thick-colored dashed lines are the linear fits of the correlation coefficients while the thin-black dashed line corresponds to the threshold of 0.9 used for detecting collinearity problems.

Fig. 6 shows the matching between the measurements and outputs for output-error approaches. The maneuver refers to a pitch doublet conducted at J = 0.331.

From the top to the bottom subplot, the figure displays the true airspeed (TAS) \mathcal{V} , the angle of attack α , the pitch rate q, the pitch angle θ and the deflection of the elevator δe . Blue lines refer to the flight data whereas the red and yellow lines to the outputs computed with the aerodynamic model estimated through the equation error and the output error approaches respectively.

The matching between outputs and measurements appears satisfactory already for the model identified with the equation error. The model estimated through the output error, on the other hand, features an improved agreement, visible in all outputs especially between 0.5 and 1.5 seconds when the elevator perturbation takes place.

Finally, Fig. 7 shows the S&C derivatives, estimated with the output error, for all the analyzed maneuvers versus the advance ratio. Again, the values for $J = \infty$ represent the unblown coefficients, while

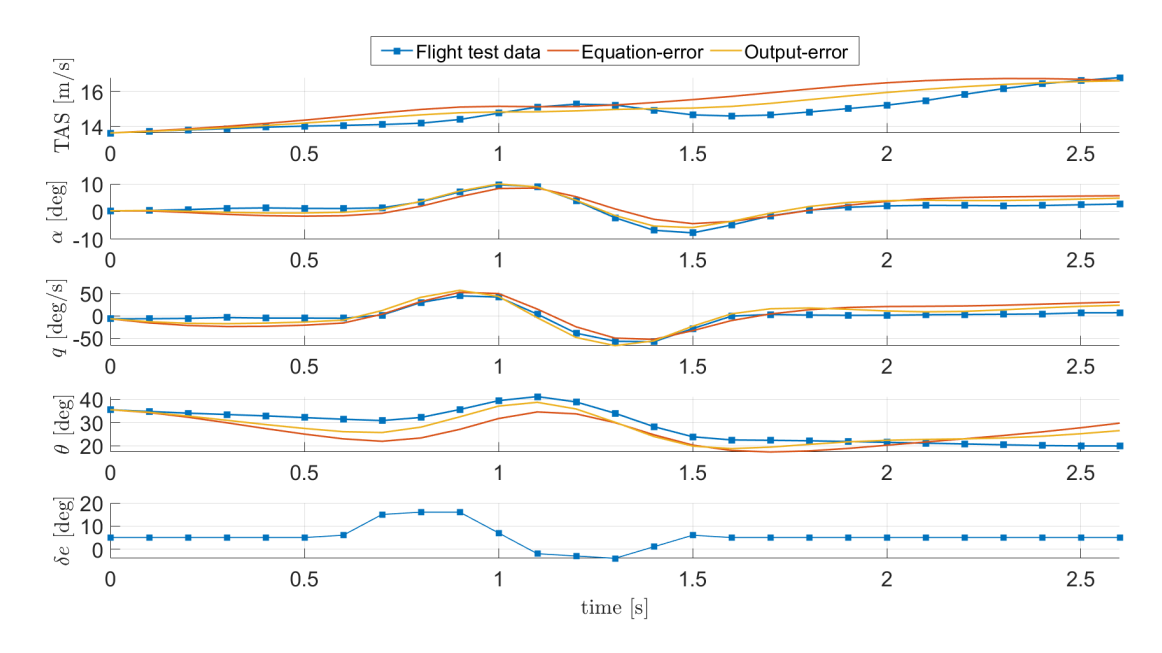


Figure 6 – Agreement between flight and simulated data for a pitch doublet at 15 m/s and advance ratio J=0.331. Top plot: true airspeed (TAS); second plot: angle of attack α ; third plot: pitch rate q; fourth plot: pitch angle θ ; bottom plot: elevator deflection δe .

the red lines indicate the exponential fitting curves that can be extracted from such data. The error bars refer to the standard deviation computed through the Cramèr-Rao lower bounds according to Eq. (25).

According to the results, only some stability derivatives feature a clear exponential trend as predicted by the vortex lattice method implemented in OpenVSP. Those are the reference coefficients, C_{Lref} , C_{Dref} and C_{mref} and the lift and moment derivatives with respect to the pitch rate, $C_{L\hat{q}}$ and $C_{m\hat{q}}$. Moreover, among the control derivatives, only $C_{m\delta e}$ seems significantly affected by blowing. The blowing either not or mildly influences the rest of the derivatives.

The fact that, via flight testings, we found that the blowing influences only a limited set of S&C derivatives, whereas <code>OpenVSP</code> predicted an impact on all parameters, deserves further investigation. At first sight, it may indicate that the actuator disk model implemented in <code>OpenVSP</code> could not accurately capture the complex aero-propulsive interaction involved in the DEP demonstrator. Additionally, some constructive details of the AeroSwitch airplane and manufacturing imperfections, that are not present in the vortex lattice model, could play an important aerodynamic role, especially when it comes to considering scaled demonstrators. Last, but not least, the identification process, being based on noisy measurements, is on its own associated with a certain level of uncertainty, and consequently, may miss some minor effects of the blowing.

At the present status of the work, it is hard to find a consolidated reason for the mismatch between vortex lattice predictions and the results identified from the flight data, although our opinion is that the results obtained from the testing campaign are the most reliable ones.

A close inspection of the identified trends, displayed in Fig. 7, allows us to derive additional conclusions

In particular, looking at the static stability coefficients, it seems that only the reference coefficients $(C_{Lref}, C_{Dref} \text{ and } C_{mref})$ are affected by blowing, while the α -derivatives do not seem to be significantly influenced. This behavior vaguely resembles the impact of a high-lift device based on trailing edge flaps.

Among the derivative with respect to the nondimensional pitch rate \hat{q} , $C_{L\hat{q}}$ and $C_{m\hat{q}}$ features an important dependence on J. In particular, the value of damping-in-pitch $C_{m\hat{q}}$ at J=0.31 is four times that of the unblown case for $J=\infty$; an indication that suggests that high blowing levels may entail increase in the damping of the short period mode. Looking again at the $C_{m\hat{q}}$ derivative, it is possible to notice, especially for $J\geq 0.5$ (low blowing conditions), that some positive values of the damping in pitch were found, representing nonrealistic estimates. A similar discussion can be done for $C_{L\hat{q}}$ derivative, which

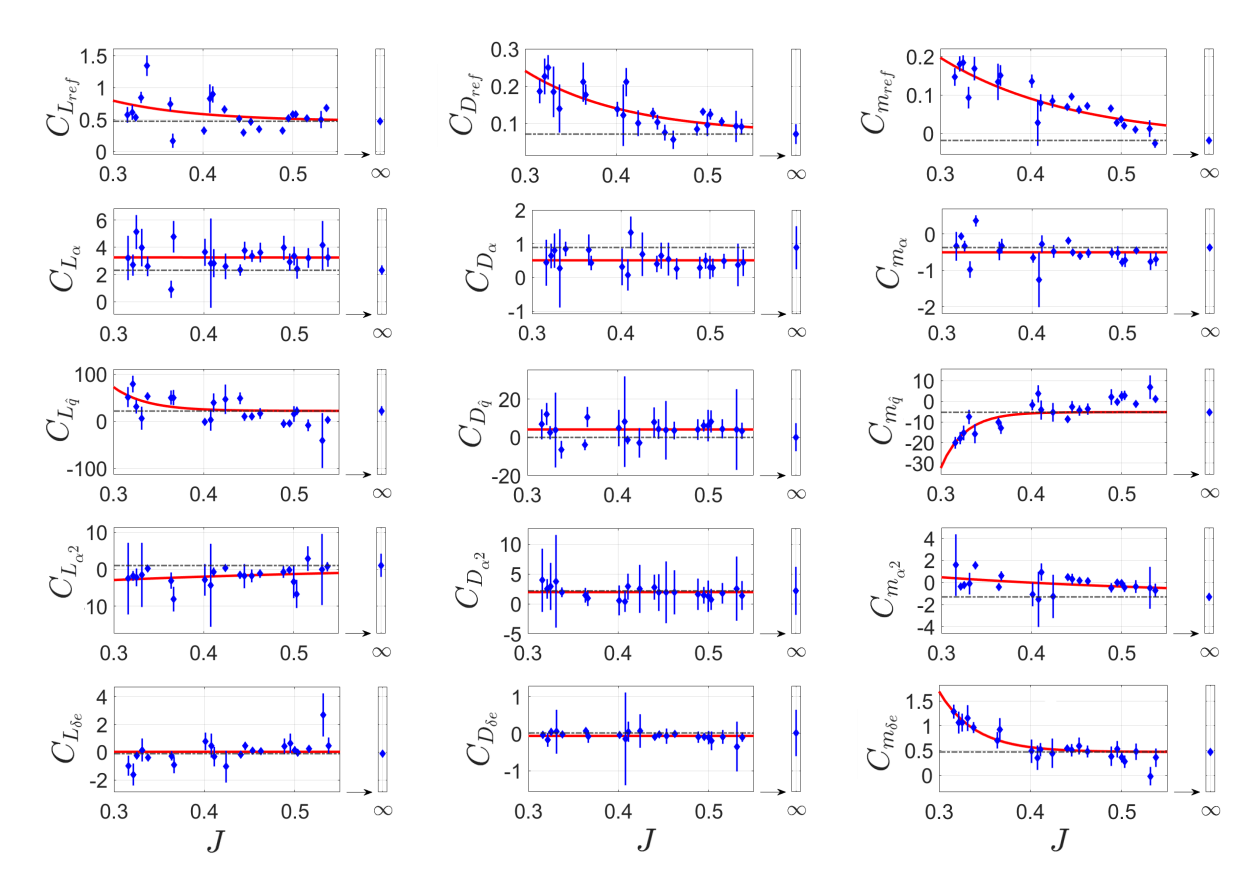


Figure 7 – Estimated S&C derivatives as functions of the advance ratio *J* and associated exponential trend. Blue markers: estimated derivatives; error bars: standard deviation of estimated quantities; Black dash-dotted line: unblown coefficients.

shows non-reliable negative estimates for some high advance rations. This fact is probably due to the poor statistical metrics associated with some of the tests, as highlighted when commenting on the collinearity of the regressors (see Fig. 5), where we have already noticed a possible collinearity issue between δe and q regressors. This possibly indicates that for $J \geq 0.5$ the estimates for some S&C derivatives are unreliable.

Dealing with control derivatives, $C_{m\delta e}$ represents the most affected by blowing. In this particular case, the exponential trend is quite evident already in the estimated derivatives, even though the scatter appears large for $J \geq 0.5$. This fact, again, is due to the poor statistical properties of the tests conducted at high J, as previously observed for $C_{L\hat{q}}$ and $C_{m\hat{q}}$ derivatives.

Finally, looking globally at the trends of the aerodynamic parameters, it is possible to notice that, while the reference parameters, C_{Lref} , C_{Dref} and C_{mref} , are influenced by the blowing also for high advance ratios, the S&C derivatives are typically affected only up to J=0.4. Beyond J=0.4 the derivatives assume values close to the unblown case.

4. Conclusions

This paper deals with the preliminary identification of the stability and control derivatives from flight data of a model aircraft featuring distributed electrical propulsion, named SwitchMaster. The focus of this work is on modeling the impact of the propeller blowing on the aerodynamic derivatives.

At first, a reference SwitchMaster model was developed within a vortex lattice code implementing the actuator disk formulation to render the effects of the propellers. From a preliminary analysis, it was possible to observe the behavior of the stability and control derivatives as functions of the propeller advance ratio. In particular, it was observed that the blowing affects the entire set of stability and control derivatives in a wide range of advance ratios, i.e. till J=0.5. Moreover, the variation of most of the stability and control derivatives in terms of the propeller advance ratio can be modeled through an exponential function.

Afterward, an intensive flight testing campaign was performed with the goal of providing the data for estimating the stability and control derivatives of the SwitchMaster for different propeller advance ratios, and hence, for suitably describing the complex aero-propulsive interaction characterizing these typologies of airplanes.

Finally, the stability and control derivatives were estimated through the standard equation- and outputerror approaches, providing the first version of the flight mechanics model of the SwithMaster.

From the analyses of the flight data and the estimation of the stability and control derivatives, it is possible to derive the following comments:

- To identify the aerodynamic model including the blowing impact, several tests have to be performed, providing that a suitable variation of the advance ratio is spanned within the tests. This often implies flight conditions at high climb angles. In particular, the Switch Master experienced climb angles close to 40 deg when it was tested at the lowest advance ratios.
- From the identified aerodynamics, it appears that only some of the stability and control derivatives are strongly affected by the blowing. This is partially in contrast with the simulations performed through a vortex lattice method, which predicted a significant impact on all derivatives.
- If we focus on the parameters mostly affected by the blowing, it can be seen that the exponential function is appropriate to capture the aero-propulsive interaction in terms of the advance ratio, as also noticed in the vortex lattice simulation.
- For the SwitchMaster airplane, analyzed here, we observed that the blowing is important till J=0.4, then, beyond that value, the derivatives are not significantly influenced. This fact represents an additional discrepancy between the flight data and vortex lattice simulations, that predicted a wider range (till J=0.5) associated with a noticeable impact of blowing.
- In general, the blowing may have a strong impact on the stability and control derivatives of the airplane, and hence also on its stability and controllability. In particular, we observed that, along with the reference coefficients, i.e. C_{Lref} , C_{Dref} and C_{mref} , also $C_{m\delta e}$ and $C_{m\hat{q}}$ feature a significant variability with J.

Clearly, this work represents only the first step toward an overall flight mechanics characterization of the complex aero-propulsive interaction involved in a DEP demonstrator. From this experimentation, some lessons were learned. In particular, for identification purposes, the pilot must have feedback from the airplane to understand if the system is trimmed and if the modes are suitably excited. In this context, an automatic way to trim and perturb the SwitchMaster appears to be a solution to ease test execution and to improve the goodness of the obtained data.

The definition and the implementation of an automatic altitude- and speed-hold controller, based on total energy control [15], is currently under development [16] and will be used in the next flight campaign.

5. Contact Author Email Address

Authors' contacts: Stefano Cacciola (stefano.cacciola@polimi.it, corresponding author), Lorenzo Trainelli (lorenzo.trainelli@polimi.it), Carlo E. D. Riboldi (carlo.riboldi@polimi.it).

6. Copyright Statement

The authors confirm that they, and/or their company or organization, hold copyright on all of the original material included in this paper. The authors also confirm that they have obtained permission, from the copyright holder of any third party material included in this paper, to publish it as part of their paper. The authors confirm that they give permission, or have obtained permission from the copyright holder of this paper, for the publication and distribution of this paper as part of the ICAS proceedings or as individual off-prints from the proceedings.

7. Acknowledgements

The authors first acknowledge the contribution of Davide Pasquali M.Sc. who accomplished the hard task of piloting the SwitchMaster during this testing campaign, and would also like to thank Lorenzo Germinario M.Sc., who supported the testing campaign and the data analysis.

References

- [1] Patterson M D, Derlaga J M and Borer N K. High-lift propeller system configuration selection for NASA's SCEPTOR distributed electric propulsion flight demonstrator. *16th AIAA Aviation Technology, Integration, and Operations Conference*, pp 1–19, 2016. https://doi.org/10.2514/6.2016-3922.
- [2] Airbus, Daher and Safran. Ecopulse A new approach to distributed propulsion for aircraft. Web page: https://www.airbus.com/en/innovation/low-carbon-aviation/hybrid-and-electric-flight/ecopulse. Last access: 3 May 2024.
- [3] Pasquali D, Santeramo A, Alberti L, Tombolini M, Trainelli L and Riboldi C E D. Distributed Electric Propulsion Aircraft Simulating a Single Propeller Aircraft. European Patent application PCT/EP2021/06217, November 14, 2016.
- [4] Trainelli L, Riboldi C E D and Cacciola S. Design, Implementation and Testing of a Distributed Electric Propulsion Demonstrator. *34th Society of Flight Test Engineers European Chapter Symposium (SFTE-EC 2023)*, pp 1–11, Roma, Italy, May 16–18, 2023.
- [5] McDonald R A and Gloudemans J R. Open Vehicle Sketch Pad: An Open Source Parametric Geometry and Analysis Tool for Conceptual Aircraft Design. *AIAA SCITECH 2022 Forum*, pp. 1–32, San Diego, CA, USA, January 3–7, 2022. https://doi.org/10.2514/6.2022-0004.
- [6] Kim H D, Perry A T and Ansell P J. A Review of Distributed Electric Propulsion Concepts for Air Vehicle Technology. AIAA/IEEE Electric Aircraft Technologies Symposium (EATS), pp. 1–21, Cincinnati, OH, USA, July 9–11, 2018.
- [7] Brelje B J and Martins J R R A. Electric, hybrid, and turboelectric fixed-wing aircraft: A review of concepts, models, and design approaches. *Progress in Aerospace Sciences*, Vol. 104, pp. 1–17, 2019. https://doi.org/10.1016/j.paerosci.2018.06.004.
- [8] Ciliberti D, Benard E, and Nicolosi F. Benchmark of different aerodynamic solvers on wing aero-propulsive interactions. *IOP Conference Series: Materials Science and Engineering*, Vol. 1226 No. 1, Paper No. 012008, 2022. https://dx.doi.org/10.1088/1757-899X/1226/1/012008.
- [9] de Vries R, Brown M and Vos R. Preliminary sizing method for hybrid-electric distributed-propulsion aircraft. *Journal of Aircraft*, Vol. 56, No. 6, pp. 2172—2188, 2019. https://doi.org/10.2514/1.C035388.
- [10] Hoogreef M F M, de Vries R, Sinnige T and Vos R. Synthesis of aero-propulsive interaction studies applied to conceptual hybrid-electric aircraft design. AIAA Scitech 2020 Forum, Orlando, FL, USA, January 6–10 , 2020. https://doi.org/10.2514/6.2020-0503.
- [11] Alberti L. AeroSwitch project: development of the flight simulator of a distributed electric propulsion demonstrator. M.Sc. thesis, Politecnico di Milano, Milan, Italy. June 9, 2021. https://hdl.handle.net/10589/176119.
- [12] Bottà L. *Modeling and identification of a distributed electric propulsion demonstrator aircraft.* M.Sc. thesis, Politecnico di Milano, Milan, Italy. July 18, 2023. https://hdl.handle.net/10589/209328.
- [13] Patterson M D, Derlaga J M and Borer N K. High-Lift Propeller System Configuration Selection for NASA's SCEPTOR Distributed Electric Propulsion Flight Demonstrator, *AIAA 2016. 16th AIAA Aviation Technology, Integration, and Operations Conference*. Washington, D.C., USA, 13–17, 2016. https://doi.org/10.2514/6.2016-3922.
- [14] Klein V and Morelli E A. *Aircraft System Identification: Theory and Practice*. AIAA, Education Series, Reston, VA, USA, 2006.
- [15] Faleiro L F and Lambregts A A. Analysis and tuning of a 'Total Energy Control System' control law using eigenstructure assignment. *Aerospace Science and Technology* Vol. 3, No. 3, pp. 127—140, 1999.
- [16] Germinario L. *Identification of the aerodynamics of a distributed electric propulsion demonstrator: towards the definition of a fully automated testing campaign*. M.Sc. thesis, Politecnico di Milano, Milan, Italy. April 9, 2024. https://hdl.handle.net/10589/219028.